

Antisymmetric Spin-Orbit Coupling Effect on Kondo-Induced Electric Polarization in a Triangular Triple Quantum Dot

Mikito Koga¹, Masashige Matsumoto², and Hiroaki Kusunose³

¹*Department of Physics, Faculty of Education, Shizuoka University, Shizuoka 422-8529, Japan*

²*Department of Physics, Faculty of Science, Shizuoka University, Shizuoka 422-8529, Japan*

³*Department of Physics, Meiji University, Kawasaki 214-8571, Japan*

We study the local antisymmetric spin-orbit (ASO) coupling effect on spin, orbital, and charge degrees of freedom for the Kondo effect in a triangular triple quantum dot (TTQD). Here, one of the three QDs is coupled to a metallic lead through electron tunneling, and a local electric polarization is induced by the Kondo effect. The ASO interaction is introduced in the other two coupled QDs on the opposite side of the lead. Generally, the ASO coupling effect is very weak and not easily detectable, but it essentially causes spin and charge reconfigurations in the TTQD through the Kondo effect. Using an extended Anderson model for the TTQD Kondo system, we elucidate that the ASO coupling gives rise to a considerable reduction of the emergent electric polarization, as a consequence of the parity mixing of molecular orbitals in the triangular loop as well as the spin-up and spin-down coupling of local electrons. The latter leads to a local diamagnetic susceptibility owing to the ASO coupled spins. We also show that the Kondo-induced electric polarization can be controlled by the ASO coupling as well as by the magnetic flux penetrating through the TTQD.

1. Introduction

The Kondo effect is a strongly correlated quantum phenomenon originating from a local spin coupled to conduction electrons antiferromagnetically owing to the strong repulsion between localized electrons in atomic orbitals.¹⁾ The low-temperature physics is well explained by the Fermi liquid picture, in which the local spin is completely screened by the conduction electrons through the formation of a spin singlet called the Kondo singlet. The Kondo physics has been extensively studied in a wide range of fields from *d*- or *f*-electron impurities embedded in bulk materials^{2,3)} to artificial atomic systems with metallic lead contacts such as quantum dot (QD) or magnetic molecular devices.⁴⁻⁹⁾ In particular, much attention has been paid to rich Kondo phenomena associated with coupled spin clusters or fabricated quantum devices, for instance, the transport properties between leads through a double^{4,6,10-15)} or triple QD.¹⁶⁻²⁰⁾

As a different context, several theoretical studies have recently investigated the Kondo effect for a single impurity in two-dimensional electron gas with the Rashba spin-orbit (SO) coupling.²¹⁻²⁶⁾ The Rashba coupling is one of the antisymmetric spin-orbit (ASO) interactions and has attracted much attention from numerous researchers of bulk systems, such as the spintronics in semiconductors,^{27,28)} topological insulators,^{29,30)} and non-centrosymmetric superconductors.³¹⁾ For the Rashba Kondo system, it has been found that the low-temperature physics meets the Fermi liquid picture as described by the conventional Kondo model, although the Kondo temperature can be considerably increased in certain situations for a relatively strong coupling of the Rashba SO interaction.²⁶⁾ All the above studies devoted themselves to the SO coupling effects on itinerant

or band electrons.

On the nanoscale, an ASO coupling also arises in coupled atoms with different-parity orbitals when the inversion symmetry is absent. Let us consider the transfer of tight-binding electrons between two atoms through the overlap of localized orbitals. Owing to the absence of the inversion symmetry, a local electric field gives rise to the mixing of intraatomic even- and odd-parity orbitals, leading to an effective spin and orbital exchange interaction on the electron hopping between the two sites.³²⁾ The orbital exchange occurs between symmetric-bonding and antisymmetric-bonding states of the coupled atoms, which resembles the antisymmetric \mathbf{k} dependence of the ASO interactions in bulk systems, where \mathbf{k} is the wave vector of an itinerant electron. It is expected that this ASO interaction plays an important role in the parity mixing of degenerate molecular orbitals in coupled magnetic impurities such as a triangular triple quantum dot (TTQD).

For the last decade, the TTQD has been experimentally realized in AlGaAs/GaAs heterostructures³³⁻³⁷⁾ and self-assembled InAs systems.³⁸⁾ The recent development of a fabrication technique has stimulated theoretical investigations of various TTQD Kondo systems because of the high potentiality for versatile quantum devices.³⁹⁻⁵¹⁾ The tunable parameters in the TTQD are interdot electron-hopping matrix elements and intradot orbital energy levels used as a standard theoretical setup. The electron occupation number at each dot changes with the depth of the orbital energy relative to the Coulomb coupling. In particular, in a half-filled case, the three-site spins are coupled antiferromagnetically owing to the superexchange process between two sites with opposite spins. This spin frustration competes with the

Kondo effect and leads to a quantum transition associated with the stabilization or destabilization of Kondo singlet formation, which was investigated for several configurations of dot-lead contacts.^{42–44, 47, 48, 50} The loop structure of the TTQD also gives rise to interference effects such as the Aharonov–Bohm (AB) effect,^{10, 52–56} where a magnetic flux penetrating through the loop affects the molecular orbitals of the TTQD and modifies the Kondo behavior in the absence of a magnetic field.^{39, 43} However, most of the theoretical studies have mainly focused on the conductance through the TTQD as an observable and controllable physical quantity.

As mentioned above, the parity mixing of molecular orbitals is another important feature of the closed loop of the TTQD.^{57, 58} The charge number at each site is closely correlated with the three-site spin configuration, and the deviation of charge depends on the third order of the intersite electron hopping parameter.⁵⁹ In this paper, we consider the local ASO coupling as a source of orbital-parity mixing and demonstrate how the parity mixing affects the electric polarization induced by the Kondo effect, as illustrated in Fig. 1 (the details are described in Sect. 3). The ASO interaction can be realized in the absence of the inversion symmetry related to the two-dimensionality of triangular arrangements of atoms or QDs. Generally, the orbital-parity mixing is not detectable since the bare value of the local ASO coupling is rather small. However, this ASO coupling affects the Kondo screening process in an essential way. When the ASO interaction is absent, the Kondo-induced electric polarization (KIEP) is generated by one of two different-parity orbitals of the TTQD strongly coupled to lead electrons in the Kondo singlet formation. For a finite ASO coupling, the other orbital also participates in the Kondo singlet and gives rise to a considerable reduction of the emergent electric polarization. Since these orbitals are coupled with spins, the local spin susceptibility exhibits a unique ASO coupling dependence. This is different from another orbital-mixing effect on the KIEP associated with the AB effect, which has been reported in our recent paper.⁶⁰ Here, we also compare the control of the electric polarization via the ASO coupling and magnetic flux to elucidate a common feature of the parity mixing of molecular orbitals in the TTQD.

This paper is organized as follows. In Sect. 2, the local ASO interaction is described in the case of coupled QD sites, and an essential role of the ASO coupling is demonstrated by a two-site Hubbard model. In Sect. 3, an extended Anderson model for the TTQD is given, which is used to investigate the interplay between the ASO coupling and Kondo effects on the emergent electric polarization, i.e., KIEP. In Sect. 4, the KIEP and local spin susceptibility are calculated as a function of a parity-mixing parameter corresponding to the ASO coupling using Wilson’s numerical renormalization group (NRG) method.^{61–63} For comparison, a similar parity-mixing effect is also shown in the presence of a magnetic flux through the triangular loop as a different context. The summary and concluding remarks are given in the last section. In Appendix A, a derivation of the local ASO interaction is shown by analogy with atomic states. In

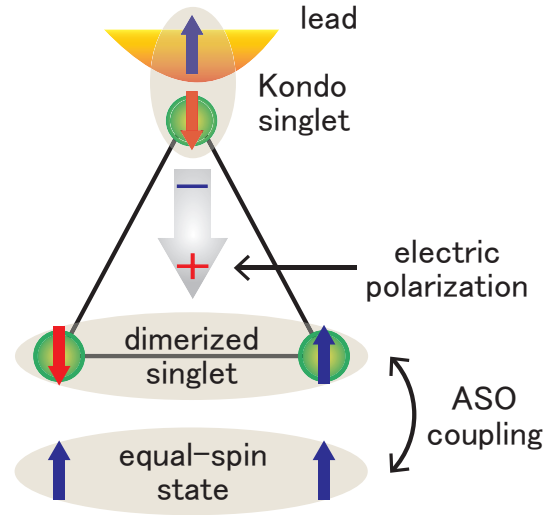


Fig. 1. (Color online) Illustration of the TTQD Kondo system. When the ASO coupling ($\lambda_A = \gamma t$) is absent, the Kondo singlet is realized at the top site (labeled a in the model), which is accompanied by a dimerized spin singlet at the bottom (b - c bond in the model). This spin reconfiguration induces charge redistribution in the TTQD and electric polarization (KIEP) at low temperatures (represented by the arrow at the center of the triangle). The local ASO coupling introduced in the b - c bond causes an effective spin and orbital exchange as well as parity mixing of the E_{\pm} molecular orbitals, which leads to a considerable reduction of the electric polarization for a small Kondo coupling strength. Simultaneously, equal-spin states with $S_z = \pm 1$ are mixed with the b - c singlet in the ground state and this mixing weight is increased by the ASO coupling.

Appendix B, the lowest-energy states of a TTQD are described in a half-filled case of a three-site Hubbard model, which is used to explain the ASO coupling effect on KIEP in Sect. 4. Appendix C gives a brief review of the magnetic flux effect on an isolated TTQD.

2. Local Antisymmetric Spin-Orbit Interaction

First, we consider an ASO interaction between two sites labeled 1 and 2 as expressed by the following Hamiltonian:

$$H_{\text{so}}(1, 2) = \lambda_A (d_{1\uparrow}^\dagger d_{2\downarrow} - d_{2\uparrow}^\dagger d_{1\downarrow} - d_{1\downarrow}^\dagger d_{2\uparrow} + d_{2\downarrow}^\dagger d_{1\uparrow}), \quad (1)$$

where $d_{i\sigma}^\dagger$ ($d_{i\sigma}$) is a creation (annihilation) operator for a localized electron at the i th site with spin σ ($=\uparrow, \downarrow$) and λ_A is a coupling constant. This local interaction can be derived by onsite and intersite hybridizations between different-parity atomic orbitals in addition to an onsite SO interaction between degenerate orbitals.⁶⁴ As described in Appendix A, it becomes relevant for multi-orbital electron systems in the absence of the inversion symmetry, which resembles the ASO interactions of band electrons in two-dimensional systems. For simplicity, we have assumed that the two sites are aligned in the x direction and the intersite orbital-parity mixing is owing to a deviation from the inversion symmetry in the z direction. In the two-site electron system, we define the even-parity (symmetric-bonding) and odd-parity (antisymmetric-bonding) orbital electrons with new op-

erators as

$$d_{e\sigma}^\dagger = \frac{d_{1\sigma}^\dagger + d_{2\sigma}^\dagger}{\sqrt{2}}, \quad d_{o\sigma}^\dagger = \frac{d_{1\sigma}^\dagger - d_{2\sigma}^\dagger}{\sqrt{2}}, \quad (2)$$

respectively, since they are transformed as $d_{e\sigma}^\dagger \rightarrow d_{e\sigma}^\dagger$ and $d_{o\sigma}^\dagger \rightarrow -d_{o\sigma}^\dagger$ with respect to the interchange of the site indices $1 \leftrightarrow 2$. Using the orbital basis in Eq. (2), Eq. (1) is rewritten as

$$H_{\text{so}} = \lambda_A (-d_{e\uparrow}^\dagger d_{o\downarrow} + d_{o\uparrow}^\dagger d_{e\downarrow} + d_{e\downarrow}^\dagger d_{o\uparrow} - d_{o\downarrow}^\dagger d_{e\uparrow}). \quad (3)$$

Using pseudospin components $\tau = \uparrow$ and $\tau = \downarrow$ for the orbital indices 'e' and 'o', respectively, the spin and orbital exchange in Eq. (3) is simplified to

$$H_{\text{so}} = \lambda_A \sum_{\tau\tau'\sigma\sigma'} d_{\tau\sigma}^\dagger (\tau_y)_{\tau\tau'} (\sigma_y)_{\sigma\sigma'} d_{\tau'\sigma'}, \quad (4)$$

where σ_y and τ_y are the y components of the Pauli matrices. The $\tau_y \sigma_y$ interaction does not conserve the z component of composite spins of the two-site electrons. Instead, the spin and orbitally coupled states are classified by

$$\eta_z = \prod_{n=1}^N (\tau_z \sigma_z)_n = \pm 1 \quad (5)$$

for N electrons, and each $(\tau_z \sigma_z)_n$ takes a value of either $+1$ or -1 for the n th electron state with $\tau, \sigma = \uparrow, \downarrow$.⁶⁵⁾ We categorize the vacuum state into $\eta_z = +1$.

Let us demonstrate how different spin states of electrons are coupled via the ASO interaction using the two-site Hubbard model

$$H_{\text{dimer}} = U(n_{1\uparrow}n_{1\downarrow} + n_{2\uparrow}n_{2\downarrow}) - t \sum_{\sigma} (d_{1\sigma}^\dagger d_{2\sigma} + d_{2\sigma}^\dagger d_{1\sigma}) + H_{\text{so}}(1, 2), \quad (6)$$

where $n_{i\sigma}$ ($\equiv d_{i\sigma}^\dagger d_{i\sigma}$) represents the number of i th-site electrons with σ , U (> 0) is the Coulomb coupling, and t (> 0) is the electron-hopping matrix element between the two sites. At half-filling, we consider the lowest-energy state for $t/U \ll 1$ dominated by the following spin-singlet state:

$$|\phi_S\rangle = \frac{1}{\sqrt{2}} (d_{1\uparrow}^\dagger d_{2\downarrow}^\dagger - d_{1\downarrow}^\dagger d_{2\uparrow}^\dagger) |0\rangle, \quad (7)$$

where $|0\rangle$ represents a vacuum state. This is combined with the doubly occupied state

$$|\phi_D\rangle = \frac{1}{\sqrt{2}} (d_{1\uparrow}^\dagger d_{1\downarrow}^\dagger + d_{2\uparrow}^\dagger d_{2\downarrow}^\dagger) |0\rangle \quad (8)$$

through the transition matrix element $\langle \phi_D | H_{\text{dimer}} | \phi_S \rangle = -2t$. Both states are categorized into the $\eta_z = -1$ type. Indeed, their orbital-basis wave functions are given as

$$|\phi_S\rangle = \frac{1}{\sqrt{2}} (d_{e\uparrow}^\dagger d_{e\downarrow}^\dagger - d_{o\uparrow}^\dagger d_{o\downarrow}^\dagger) |0\rangle, \\ |\phi_D\rangle = \frac{1}{\sqrt{2}} (d_{e\uparrow}^\dagger d_{e\downarrow}^\dagger + d_{o\uparrow}^\dagger d_{o\downarrow}^\dagger) |0\rangle. \quad (9)$$

One can find that the doubly occupied (e, \uparrow) and (e, \downarrow) electron states lead to $\eta_z = (\tau_z \sigma_z)_{e\uparrow} \times (\tau_z \sigma_z)_{e\downarrow} = (+1) \times (-1) = -1$. The same algebra is also applied to (o, \downarrow) with $\tau_z \sigma_z = +1$ and (o, \uparrow) with $\tau_z \sigma_z = -1$. When λ_A is finite, $|\phi_D\rangle$ is coupled to an equal-spin state (y

component of a spin-triplet state) with $\eta_z = -1$,

$$-i|\phi_{T_y}\rangle = \frac{1}{\sqrt{2}} (d_{1\uparrow}^\dagger d_{2\uparrow}^\dagger + d_{1\downarrow}^\dagger d_{2\downarrow}^\dagger) |0\rangle \\ = \frac{1}{\sqrt{2}} (d_{o\uparrow}^\dagger d_{e\uparrow}^\dagger + d_{o\downarrow}^\dagger d_{e\downarrow}^\dagger) |0\rangle, \quad (10)$$

through $i\langle \phi_{T_y} | H_{\text{dimer}} | \phi_D \rangle = -\lambda_A$. On the basis of the above three states, the diagonal matrix elements of H_{dimer} are as follows:

$$\langle \phi_S | H_{\text{dimer}} | \phi_S \rangle = \langle \phi_{T_y} | H_{\text{dimer}} | \phi_{T_y} \rangle = 0, \\ \langle \phi_D | H_{\text{dimer}} | \phi_D \rangle = U. \quad (11)$$

After diagonalizing the 3×3 matrix of H_{dimer} , we obtain the lowest-energy state

$$|\psi_g\rangle \simeq \frac{1-\delta}{\sqrt{1+\gamma^2}} |\phi_S\rangle + 2\bar{t}\sqrt{1+\gamma^2} |\phi_D\rangle \\ + \frac{\gamma(1-\delta)}{\sqrt{1+\gamma^2}} (-i) |\phi_{T_y}\rangle, \quad (12)$$

which is solved up to the second order of \bar{t} ($\equiv t/U$), where γ ($\equiv \lambda_A/t$) is used and $\delta = 2\bar{t}^2(1+\gamma^2)$. Thus, the different spin states $|\phi_S\rangle$ with $S_z = 0$ and $-i|\phi_{T_y}\rangle$ with $S_z = \pm 1$ are coupled to each other by the ASO interaction through $|\phi_D\rangle$. As a consequence, the vector spin chirality $\langle \psi_g | (\mathbf{S}_1 \times \mathbf{S}_2)_y | \psi_g \rangle \simeq \gamma/(1+\gamma^2)$ is generated, where \mathbf{S}_i ($i = 1, 2$) is the spin operator ($\mathbf{S} \equiv \boldsymbol{\sigma}/2$) at the i th site.⁶⁶⁾ This is closely related to the emergent electric polarization due to the mixing of different-parity orbitals in the absence of the inversion symmetry.⁶⁷⁾

For the later calculation, we also show the roles of the ASO coupling in a half-filled three-site Hubbard model for the strong Coulomb coupling $\bar{t} \ll 1$ in Appendix B. As in the above two-site case, the ASO coupled spins generate a vector spin chirality perpendicular to the axis along which the two spins are aligned.

3. Model

To elucidate the role of the ASO interaction in strongly correlated electron systems, we study the Kondo effect in the TTQD, where one of the three sites is connected to a metallic lead through electron tunneling. In such an artificial molecule, spin and charge reconfigurations are generated by the Kondo effect. This nanoscale magnetoelectric effect can be controlled by an intersite ASO interaction in the spin cluster if the ASO coupling strength is tunable. For instance, the coupling constant λ_A in Eq. (1), namely, γ in Eq. (A.14), depends on the on-site and intersite orbital-parity mixing V_z and t_{sp} , respectively. The former is associated with the absence of the inversion symmetry that induces a local electric field in the z direction,⁶⁴⁾ which can be fine-tuned by gate-voltage control in nanoscale devices. Here, we introduce the ASO interaction in only one bond of the TTQD on the opposite side of the lead, which breaks the equivalency of the three QDs. However, point-group representations of the triangular symmetry are still useful for classifying local electron states of the TTQD. As a major advantage of this simplification, we can demonstrate more clearly the interplay between the ASO coupling

and Kondo effects through the different-parity mixing of molecular orbitals in the TTQD, since the local ASO interaction does not affect the Kondo effect directly and can be regarded as a moderate perturbation.

We investigate the above ASO coupling effect using an extended Anderson model Hamiltonian that consists of three terms, $H = H_d + H_1 + H_{1-d}$, for the TTQD, the kinetic energy of lead electrons, and the electron tunneling, respectively. The first term is represented by the following Hubbard-type model frequently used for the TTQD:

$$H_d = -t \sum_{i \neq j} \sum_{\sigma} d_{i\sigma}^{\dagger} d_{j\sigma} + \sum_i \left(\varepsilon_d + \frac{U}{2} \right) n_i + \frac{U}{2} \sum_i (n_i - 1)^2 + H_{so}(b, c) \quad (i, j = a, b, c). \quad (13)$$

Here, the three sites are identical, except for the presence of the ASO interaction in Eq. (1) between the b - and c -sites. The onsite electron number n_i ($\equiv n_{i\uparrow} + n_{i\downarrow}$) depends on the depth of the local orbital energy ε_d (< 0). Here, we choose the symmetric condition $\varepsilon_d = -U/2$ that favors single-electron occupation at each site and generates a local spin. In the lead-electron term

$$H_1 = \sum_{\mathbf{k}\sigma} \varepsilon_{\mathbf{k}} c_{\mathbf{k}\sigma}^{\dagger} c_{\mathbf{k}\sigma}, \quad (14)$$

the creation (annihilation) of conduction electrons is represented by $c_{\mathbf{k}}^{\dagger}$ ($c_{\mathbf{k}}$) with the wave number \mathbf{k} and spin σ . We consider the electron tunneling between one of the three sites (a -site) and the lead (hybridization between the a -site orbital and a conduction band) as

$$H_{1-d} = \sum_{\mathbf{k}\sigma} (v_{\mathbf{k}} d_{a\sigma}^{\dagger} c_{\mathbf{k}\sigma} + \text{h.c.}), \quad (15)$$

where $v_{\mathbf{k}}$ is related to the level broadening of $\Gamma \equiv \pi\rho|v_{\mathbf{k}}|^2$ (ρ is the density of electron states at the Fermi energy), which is considered as a constant. As mentioned in the previous section, the total S_z is not conserved by the ASO interaction. Instead, the even or odd symmetry in terms of $\eta_z = \pm 1$ in Eq. (5) is useful for classification of the spin and orbitally coupled states. Since the lead is only connected to the a -site, the relevant conduction electrons belong to the same $\tau_z\sigma_z$ types of a -site electrons, namely,

$$c_{\mathbf{k}\uparrow}^{\dagger} \rightarrow \tau_z\sigma_z = +1, \quad c_{\mathbf{k}\downarrow}^{\dagger} \rightarrow \tau_z\sigma_z = -1. \quad (16)$$

In the present study, we calculate the electric polarization in the triangular cluster defined as

$$\begin{aligned} \delta n &= \frac{1}{3}(2\langle n_a \rangle - \langle n_b \rangle - \langle n_c \rangle) \\ &= \frac{1}{3}(2\langle n_a \rangle - \langle n_e \rangle - \langle n_o \rangle), \end{aligned} \quad (17)$$

where $\langle \dots \rangle$ represents the expectation value. The electron number in the even-parity orbital (n_e) or odd-parity orbital (n_o) is defined as $n_{\tau} = \sum_{\sigma} d_{\tau\sigma}^{\dagger} d_{\tau\sigma}$ ($\tau = e, o$), where $d_{e\sigma}^{\dagger} = (d_{b,\sigma}^{\dagger} + d_{c,\sigma}^{\dagger})/\sqrt{2}$ and $d_{o\sigma}^{\dagger} = (d_{b,\sigma}^{\dagger} - d_{c,\sigma}^{\dagger})/\sqrt{2}$. For the isolated TTQD ($\Gamma = 0$), each of the lowest-energy states in Eq. (B-9) gives the opposite expectation value to the corresponding electric polarization operator rep-

resented by $\delta \hat{n} = (2n_a - n_b - n_c)/3$ as^{57, 59)}

$$\langle \psi_{\sigma}^{E+} | \delta \hat{n} | \psi_{\sigma}^{E+} \rangle = -\langle \psi_{\sigma}^{E-} | \delta \hat{n} | \psi_{\sigma}^{E-} \rangle = 12 \left(\frac{t}{U} \right)^3. \quad (18)$$

The E_{\pm} degeneracy causes cancellation of the net electric polarization and leads to $\delta n = 0$. Thus, the appearance of a finite δn is associated with the energy difference between the E_{\pm} states. For a finite γ , the opposite-spin state $|\psi_{-\sigma}^{E-}\rangle$ is coupled to $|\psi_{\sigma}^{E+}\rangle$. When the E_+ state is considerably lowered in energy by the Kondo effect, the A_- states with the same η_z also participate in the lowest-energy state together with the E_- state as in Eq. (B-11). A schematic picture of the spin configuration is given in Fig. 1. It is expected that this ASO interaction affects the emergence of δn and gives rise to a spin reconfiguration in the TTQD, the details of which are shown by the NRG analysis in the next section.

In the NRG calculation, the logarithmic discretization parameter $\Lambda = 3$ is used for the conduction band, the half width of which is chosen as the energy unit.^{61, 62)} The physical temperature T is also measured in terms of this unit. Here, the NRG results are shown for a strong Coulomb coupling that is fixed at $U = 0.9$. At each renormalization step, about 2000 low-lying states are retained. All wave functions are classified using $\eta_z = \pm 1$ in Eq. (5) for arbitrary electron numbers N in the lead plus the TTQD.

4. Results

4.1 Local electric polarization and magnetic susceptibility

In the previous study, we showed the KIEP in the absence of the ASO interaction ($\gamma = 0$).⁵⁷⁾ As the temperature T is decreased, δn in Eq. (17) exhibits an abrupt increase and reaches a constant value δn^* at low T . The saturation value δn^* mainly depends on t/U and monotonically increases with decreasing the Kondo coupling strength Γ/U . As Γ/U approaches zero, δn^* increases up to a maximum of $12(t/U)^3$ for $t/U \ll 1$, which corresponds to $\langle \psi_{\sigma}^{E+} | \delta \hat{n} | \psi_{\sigma}^{E+} \rangle$ at $\Gamma \rightarrow 0$ in Eq. (18), indicating that $|\psi_{\sigma}^{E+}\rangle$ is stabilized by the Kondo effect.

Figure 2 shows the ASO coupling effect on δn^* and the crossover temperature T_{cr} . For $t = 0$, the latter corresponds to the conventional Kondo temperature in the Kondo effect due to a single local spin. For a finite t , the ASO coupling γ (in the unit of t) gives rise to the spin and E_{\pm} orbital mixing, leading to a reduction of T_{cr} . The γ dependence of T_{cr} can be evaluated by a universal fitting of the local magnetic susceptibility $\chi(T)$ of the TTQD for various γ values. This χ is calculated under the assumption that the applied magnetic field is perpendicular to the TTQD, i.e., parallel to the threefold axis of the triangular symmetry. The result is that the data of $\chi/\chi(T=0)$ in Fig. 3 are unified into a universal function of the rescaled temperature T/T_{cr} . This indicates that the Kondo singlet is also realized at $T < T_{cr}$ for a finite ASO coupling.

The ASO coupling effect appears more significantly in both $\delta n^*(\gamma)$ and $T_{cr}(\gamma)$ for a smaller Γ/U . The most marked feature is the strong suppression of δn^* by weak

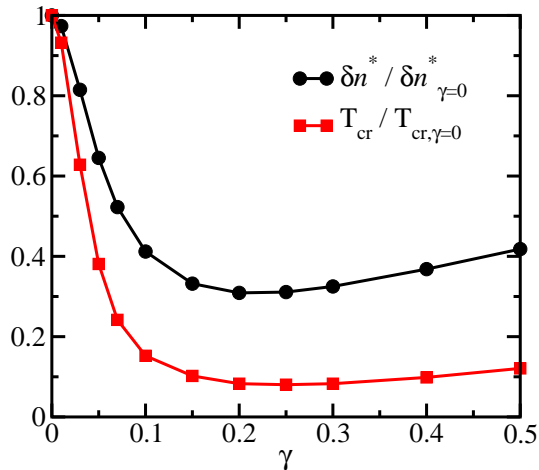


Fig. 2. (Color online) Saturation value δn^* of the emergent electric polarization at low temperatures and crossover temperature T_{cr} evaluated by the local magnetic susceptibility χ . The data normalized by each $\gamma = 0$ value are plotted as a function of γ associated with the ASO coupling strength γt for $t/U = 0.12$ and $\Gamma/U = 0.0473$.

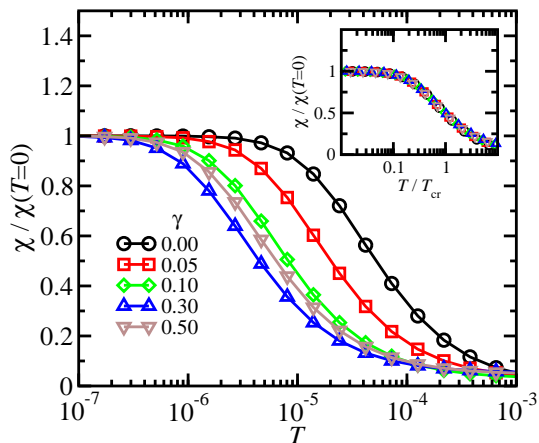


Fig. 3. (Color online) Temperature T dependence of local magnetic susceptibility of TTQD for various γ values of the ASO coupling. The data are normalized by $\chi(T = 0)$. Here, t/U and Γ/U are fixed at the same values as in Fig. 2. Inset: Universal $\chi/\chi(T = 0)$ as a function of T/T_{cr} . Here, T_{cr} is determined as the temperature for $\chi/\chi(T = 0) = 1/2$.

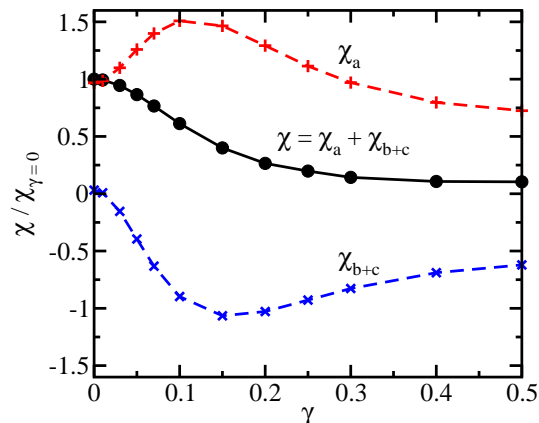


Fig. 4. (Color online) Local magnetic susceptibility of TTQD at the zero temperature $\chi = \chi_a + \chi_{b+c}$, where χ_a and χ_{b+c} are the onsite susceptibilities for the a -site and the b - plus c -sites, respectively. The data are normalized by the $\gamma = 0$ value $\chi_{\gamma=0}$ of the total χ and are plotted as a function of γ for $t/U = 0.12$ and $\Gamma/U = 0.0473$.

Table I. Relevant TTQD orbital states in the Kondo screening process, where E_+ , E_- , and A_- are the representations of wave functions in Eqs. (B-2), (B-3), and (B-4), respectively, and the orbital mixing depends on the ASO coupling γ . The KIEP δn^* exhibits an upturn at $\gamma = \gamma_{\min}$ ($\simeq 0.2$ in Fig. 2). There are three sequent γ regions characterized by δn^* and the local magnetic susceptibility: (i) Only the E_+ component participates in the Kondo screening process and gives each maximum of δn^* and $\chi = \chi_a + \chi_{b+c}$. (ii) The E_- component gives a negative contribution to δn^* , and the b - c triplet state of E_- is responsible for the diamagnetic behavior of χ_{b+c} . (iii) The mixing weight of E_- is reduced by the A_- components coupled to E_+ in the Kondo singlet, leading to a gradual increase in δn^* and decreases in $|\chi_a|$ and $|\chi_{b+c}|$.

	ASO coupling	Relevant orbitals for Kondo screening
(i)	$\gamma = 0$	E_+
(ii)	$0 < \gamma < \gamma_{\min}$	$E_+ \oplus E_-$
(iii)	$\gamma > \gamma_{\min}$	$E_+ \oplus E_- \oplus A_-$

E_{\pm} mixing for a very small γ . This indicates that $|\psi_{\sigma}^{E-}\rangle$ in Eq. (B-9) also participates in the Kondo singlet with $|\psi_{-\sigma}^{E+}\rangle$ at low T . More precisely, the spin-up conduction electrons couple with $|\psi_{\downarrow}^{E+}\rangle$ and $|\psi_{\uparrow}^{E-}\rangle$, while the spin-down conduction electrons couple with $|\psi_{\uparrow}^{E+}\rangle$ and $|\psi_{\downarrow}^{E-}\rangle$. This is a consequence of the spin and orbital coupling classified by η_z in Eq. (5). The E_+ state generates a positive electric polarization $\delta n^* > 0$ for $\gamma = 0$. In Fig. 2, the mixing weight of E_- in the ground state increases abruptly with γ (< 0.1), resulting in a negative contribution to δn^* . On the other hand, the A_- states in Eq. (B-4) give no direct contribution to δn^* but effectively reduce the mixing weight of E_- through the ASO coupling. As this A_- contribution becomes more relevant at $\gamma > 0.2$, δn^* shows a gradual increase with γ . Thus, the entire γ dependence of δn^* is explained by the orbital symmetry mixing of E_{\pm} and A_- in the ground state as summarized in Table I (also see Sect. 4.2).

In Fig. 2, T_{cr} shows a similar γ dependence to δn^* , indicating that the emergence of the electric polarization is closely associated with the Kondo effect. As mentioned above, the even-parity state $|\psi_{\sigma}^{E+}\rangle$ is only responsible for the Kondo singlet with conduction electrons at $\gamma = 0$. For a finite γ ($< \gamma_{\min} \simeq 0.2$), this Kondo coupling is weakened effectively by the ASO interaction since the odd-parity state $|\psi_{-\sigma}^{E-}\rangle$, which is not relevant to the Kondo effect, also participates in Kondo singlet formation and reduces the mixing weight of $|\psi_{\sigma}^{E+}\rangle$ in the ground state at low T (see Table I). In the b - c bonding state at $T \rightarrow 0$, a spin singlet coexists with a spin triplet as clearly shown in Fig. 4. Here, we plot χ_a for the a -site magnetic susceptibility and χ_{b+c} for the sum of the b - and c -site susceptibilities as a function of γ , in addition to the total $\chi = \chi_a + \chi_{b+c}$. For instance, let us consider that the spin "up" of the electron is parallel to the direction of the applied magnetic field. In this case, the dominant contributions to χ_a and χ_{b+c} are from $|\psi_{\uparrow}^{E+}\rangle$ and $|\psi_{\downarrow}^{E-}\rangle$, respectively. We find that the local magnetization is polarized in space, where the antiparallel local moments are generated at one apex (a -site) and the opposite side (b - c bond) of the triangular cluster. On the other hand,

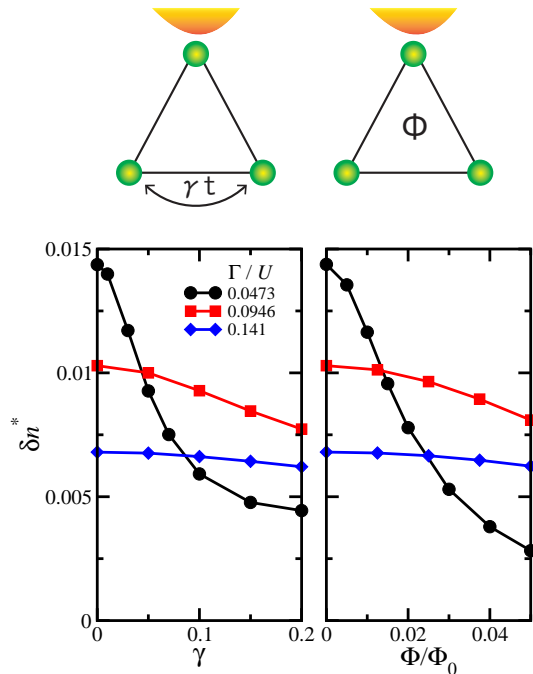


Fig. 5. (Color online) Comparison of the ASO coupling effect (left panel) with the orbital effect of a weak magnetic field (right panel) on δn^* as a function of γ and the magnetic flux Φ/Φ_0 , respectively (Φ_0 is the magnetic flux quantum). The data are for various Γ/U values, where $t/U = 0.12$ is fixed.

the total χ monotonically decreases with increasing γ . At $\gamma \simeq 0.15$, the diamagnetic χ_{b+c} exhibits an upturn and a gradual increase with γ , indicating an increase in the mixing weights of $|\phi_{3/2}^{A-}\rangle$ and $|\phi_{\downarrow}^{A-}\rangle$ in Eq. (B-4), which are coupled to $|\psi_{\uparrow}^{E+}\rangle$ as well as $|\psi_{\downarrow}^{E-}\rangle$ in the ground state.

4.2 Analogy with magnetic flux effect on orbital-parity mixing

For a small ASO coupling γ , the abrupt decrease in δn^* for a small Γ/U in Fig. 2 is well explained by the orbital-parity mixing approximately represented by $c_+|\psi_{\sigma}^{E+}\rangle + c_-|\psi_{-\sigma}^{E-}\rangle$, where c_{\pm} is the mixing weight of the E_{\pm} state. It is confirmed that the ratio $|c_-|/|c_+|$ considerably increases with γ since δn^* is proportional to $|c_+|^2 - |c_-|^2$. The KIEP δn^* is also sensitively dependent on Γ/U as shown in Fig. 5 (left). The increase in Γ/U causes the reduction of δn^* at $\gamma = 0$, and the charge distribution becomes uniform over the three sites of the triangular cluster. This indicates that the E_+ state is more dominant in the ground state, namely, $|c_-|/|c_+| \simeq 0$ for a large Kondo coupling Γ/U . In addition, the ASO coupling effect becomes irrelevant for the emergent electric polarization even when γ is larger.

For the KIEP, there is a close analogy between the above ASO coupling effect on the b - c bond and the magnetic flux effect on the orbital states in the triangular loop. Both effects give rise to the mixing of the E_{\pm} orbital parities and lead to a similar dependence of δn^* on the orbital-mixing parameters: γ for the ASO coupling and Φ/Φ_0 for the magnetic flux penetrating through the triangle in Fig. 5. The data of δn^* are plotted as a function

of each parameter for comparison. Appendix C shows the magnetic flux contribution to the wave function of the lowest-energy state for $\Gamma = 0$. When the Kondo singlet is realized at low temperatures for a finite Γ , the E_{\pm} orbital mixing for a finite Φ is expressed approximately as $c_+|\psi_{\sigma}^{E+}\rangle + c_-i|\psi_{\sigma}^{E-}\rangle$ with the conservation of the total spin S .⁶⁰⁾ On the other hand, the ASO coupling effect generates spin-up and spin-down coupling as $c_+|\psi_{\sigma}^{E+}\rangle + c_-|\psi_{-\sigma}^{E-}\rangle$ in addition to the E_{\pm} mixing, which maintains the conservation of $\eta_z = +1$ or $\eta_z = -1$. Thus, the ASO coupling γ and magnetic flux Φ effects qualitatively give the same contribution to δn^* as internal and external fields, respectively, in spite of the different orbital-parity mixing mechanisms.

5. Summary and Concluding Remarks

We have studied the local ASO coupling effect on the emergent electric polarization in a triangular cluster of magnetic impurities at low temperatures, which is relevant in the absence of the inversion symmetry. One of the three local spins in the cluster (S_a) is coupled to the lead electrons, and the ASO interaction introduced in the other coupled (b - c bond) spins causes mixing of the even and odd parities (symmetric and antisymmetric bonding) of orbital states (E_{\pm} mixing). This effect competes with the Kondo effect and gives rise to a considerable reduction of the KIEP δn^* at low temperatures for a small Kondo coupling strength Γ/U . It was also found that the ASO coupling dependence of δn^* is strongly correlated with that of the crossover temperature T_{cr} . The latter is an energy scale derived from a universal function of the low-temperature dependence of the local magnetic susceptibility. Another important result is that the ASO-coupled spins exhibit diamagnetism owing to an equal-spin pair in the odd-parity E_- state that participates in Kondo singlet formation as well as the even-parity E_+ state. We have also elucidated a close analogy between the ASO coupling and magnetic flux effects on the orbital-parity mixing as internal and external field controls of δn^* , respectively.

Here, the ASO coupling was introduced in one bond (b - c bond) of the TTQD on the opposite side of an apex connected to a lead. This side effect was considered as a kind of boundary condition for moderate control of the effective Kondo coupling with the lead electrons. Indeed, the ASO coupling strength is a controllable parameter related to the mixing weight of different-parity molecular orbitals. For instance, this partially originates from a hybridization between intradot orbitals with different parities such as the last term including V_z in Eq. (A-9), which can be induced by a local electric field in the absence of the inversion symmetry. Experimentally, the local ASO coupling can be tuned by the gate voltage and acts as a controllable boundary condition of such a Kondo system with a nanostructure.

In Sect. 2, it was pointed out that the ASO-coupled spins generate a vector spin chirality, which is closely associated with the parity mixing of the molecular orbital symmetries (here, $E_+ \oplus E_-$ and $E_+ \oplus A_-$) accompanied by spin modulation. Recently, we have reported a

group-theoretical study of various spin-dependent electric dipoles in the absence of the inversion symmetry, including the relationship between the vector spin chirality of the two-site spins and possible electric dipoles induced by a magnetic field or magnetic ordering.⁶⁷⁾ As another magnetoelectric effect, it will also be intriguing to reveal the interplay between the KIEP δn^* and the vector spin chirality generated by the ASO-coupled spins in the present model. A detailed analysis is left for a future study.

We would also like to mention a symmetry-lowering effect on δn^* , which depends on different intersite electron-hopping parameters t_{ij} ($i, j = a, b, c; i \neq j$). For the parity-symmetric case $t_{ab} = t_{ca}$ (fixed at t) in the absence of the ASO coupling, $|\phi_{\sigma,1}^{E+}\rangle$ in Eq. (B-2) is stabilized by the Kondo effect, while $|\phi_{\sigma,1}^{E-}\rangle$ in Eq. (B-3) is favored by lowering t_{bc} from t . This competition leads to a quantum transition from the former to the latter upon lowering t_{bc} . The critical point $t_c \lesssim t$ is obtained for a sufficiently small Γ/U . This quantum transition was investigated in several theoretical studies as a unique feature of the Kondo effect for a triangular loop of three magnetic impurities.^{44,47,48)} In the present study, we have focused on the KIEP in the equilateral TTQD, and the result also holds for the lower-symmetry case $t_{bc} > t_c$.

The recent development of a scanning tunneling microscope (STM) experiment has realized the manipulation of atoms and their precise arrangement in designed configurations on a surface template. Using such a fabrication technique, it is now possible to create coupled QDs with a perfect geometric structure.⁶⁸⁾ The STM image visualizes the charge distributions associated with the geometry, and the parity symmetry of a wave function is reflected in the electron density maps. In addition, STM spectroscopy unveils quantum spin configurations in artificially coupled spin chains at the atomic scale.⁶⁹⁻⁷¹⁾ Thus, it is very promising for detecting a nanoscale electric polarization correlated with local spin states, and the confirmation of the KIEP will stimulate a new application of the Kondo effect to spintronic and multiferroic devices. From a different viewpoint of the experiments, the ASO-coupling-dependent KIEP is expected to give a relevant contribution to the linear conductance between two leads through a single QD of the TTQD, which can be mapped to the present Anderson model for the TTQD with a single lead. Indeed, for a weak dot-lead contact, the ASO coupling effect causes a considerable reduction of the crossover temperature T_{cr} in Fig. 2, which corresponds to the Kondo temperature. As shown in Sect. 4.2, the ASO coupling can be considered as a magnetic flux through the TTQD and could be chosen as a controllable parameter for detecting an interference effect on the conductance, as proposed in several theoretical studies on QD systems with various configurations.^{10,39,52-56)}

This work was supported by JSPS KAKENHI Grant Numbers 16H01070 (J-Physics), 15H05885 (J-Physics), 26400332, and 15K05176.

Appendix A: Effective Spin-Orbit Interaction Due to Orbital-Parity Mixing

The ASO interaction plays an important role in electron transfer between two QDs. Here, we show a simple two-site model with different intradot orbital-parity mixing. For simplicity, we consider that even- and odd-parity orbitals are represented by, for instance, s - and p -orbitals, respectively, and the latter orbitals are coupled to spins through the SO interaction at each site as realized in real atoms. This atomlike assumption may be reasonable for local electrons strongly confined in a QD by a sort of central field, although the intradot SO coupling is extremely weak as usual. For the p -orbital wave functions, the three components $|p_x\rangle$, $|p_y\rangle$, and $|p_z\rangle$ are related to the $l = 1$ angular momentum states as

$$l_z = 1 : |p_+\rangle = \frac{1}{\sqrt{2}}(-|p_x\rangle - i|p_y\rangle), \quad (\text{A-1})$$

$$l_z = 0 : |p_z\rangle, \quad (\text{A-2})$$

$$l_z = -1 : |p_-\rangle = \frac{1}{\sqrt{2}}(|p_x\rangle - i|p_y\rangle). \quad (\text{A-3})$$

We assume that the p -orbital degeneracy is lifted by an axial crystal field and that the p_z orbital energy is much lower than that of p_x and p_y . The local p -orbital state with spin is described by the onsite Hamiltonian

$$\begin{aligned} H_p &= H_{\text{CEF}} + H_{\text{LS}} \\ &= \Delta(n_{p_x} + n_{p_y}) + \lambda \mathbf{l} \cdot \mathbf{s}, \end{aligned} \quad (\text{A-4})$$

where Δ (> 0) is the crystal-field energy measured from the p_z orbital energy level and n_{p_x} (n_{p_y}) is the number of p_x (p_y) electrons in the first term. In the second term, λ (> 0) represents the SO coupling constant and

$$\mathbf{l} \cdot \mathbf{s} = \frac{1}{2}l_+s_- + \frac{1}{2}l_-s_+ + l_zs_z, \quad (\text{A-5})$$

where for l_{\pm} ($\equiv l_x \pm il_y$), the finite matrix elements of $(l_{\pm})_{mm'}$ and $(l_z)_{mm'}$ ($m, m' = 0, \pm 1$ for l_z) are given by

$$(l_+)_{1,0} = (l_+)_{0,-1} = (l_-)_{0,1} = (l_-)_{-1,0} = \sqrt{2}, \quad (\text{A-6})$$

$$(l_z)_{1,1} = 1, \quad (l_z)_{-1,-1} = -1, \quad (\text{A-7})$$

and \mathbf{s} ($\equiv \boldsymbol{\sigma}/2$) is a spin operator ($s_{\pm} \equiv s_x \pm is_y$). For a small SO coupling $\lambda \ll \Delta$, the lowest-energy eigenstates of H_p are obtained as

$$\begin{aligned} |P, +\rangle &= |p_{z,\uparrow}\rangle - \frac{\lambda}{\sqrt{2}\Delta}|p_{+,\downarrow}\rangle, \\ |P, -\rangle &= |p_{z,\downarrow}\rangle - \frac{\lambda}{\sqrt{2}\Delta}|p_{-,\uparrow}\rangle, \end{aligned} \quad (\text{A-8})$$

with the eigenenergy $-\lambda^2/(2\Delta)$.

Next, we introduce the even- and odd-parity mixing on the basis of the s - p hybridization using the following Hamiltonian:⁶⁴⁾

$$\begin{aligned} H_{s+p} &= H_p + H_s + H_{s,p_z} \\ &= H_p - E_s n_s + V_z \sum_{\sigma} (|s, \sigma\rangle \langle p_z, \sigma| + \text{h.c.}), \end{aligned} \quad (\text{A-9})$$

where the second term with $-E_s$ (< 0) represents the energy of the s -electrons with the number operator n_s ,

and V_z in the last term represents the deviation from the inversion symmetry, namely, the hybridization strength between s - and p_z -orbitals. For a small $|V_z|$ ($\ll E_s$), the lowest-energy states of H_{s+p} are dominated by the s -electron, and the wave functions are obtained as

$$\begin{aligned} |S, +\rangle &= |s, \uparrow\rangle - \frac{V_z}{E_s} |P, +\rangle \\ &= |s, \uparrow\rangle - \frac{V_z}{E_s} |p_z, \uparrow\rangle + \frac{V_z \lambda}{\sqrt{2} E_s \Delta} |p_+, \downarrow\rangle, \\ |S, -\rangle &= |s, \downarrow\rangle - \frac{V_z}{E_s} |P, -\rangle \\ &= |s, \downarrow\rangle - \frac{V_z}{E_s} |p_z, \downarrow\rangle + \frac{V_z \lambda}{\sqrt{2} E_s \Delta} |p_-, \uparrow\rangle. \end{aligned} \quad (\text{A}\cdot 10)$$

These spin and orbitally coupled states are used for the derivation of an intersite electron hopping-type Hamiltonian. For simplicity, we assume that two sites (labeled 1 and 2) are aligned in the x direction. The position of site 1 (2) is on the left (right) side. When the electron creation and annihilation at the i th site ($i = 1, 2$) are represented by $c_{i,\mu,\sigma}^\dagger$ and $c_{i,\mu,\sigma}$, respectively, for the μ ($= s, p_+, p_-$) orbitals with spin σ , the intersite orbital mixing is described by

$$\begin{aligned} H_{\text{mix}} &= -t_{ss} \sum_{\sigma} c_{1,s,\sigma}^\dagger c_{2,s,\sigma} \\ &\quad - t_{sp} (-c_{1,s,\uparrow}^\dagger c_{2,p-\uparrow} + c_{1,p-\uparrow}^\dagger c_{2,s,\uparrow}) \\ &\quad - t_{sp} (c_{1,s,\downarrow}^\dagger c_{2,p+\downarrow} - c_{1,p+\downarrow}^\dagger c_{2,s,\downarrow}) + \text{h.c.}, \end{aligned} \quad (\text{A}\cdot 11)$$

where t_{ss} (t_{sp}) is the transition matrix element between the two-site s -orbitals (between the s -orbital on one site and the p_x -orbital on the other). We have discarded the p - p electron-hopping term since its contribution is considered to be much smaller than those of the s - s and s - p terms. The phase difference π arises in the $s \rightarrow p_x$ and $p_x \rightarrow s$ transfers between site 1 and site 2 owing to the odd parity of the p -orbital. On the basis of Eq. (A-11), we calculate the matrix elements of the overlap integrals $\langle i, S, \pm | j, S, \pm \rangle$ and $\langle i, S, \pm | j, S, \mp \rangle$ ($i, j = 1, 2$ are the site indices and $i \neq j$) in Eq. (A-10). Replacing the notations $\{+, -\}$ by $\{\uparrow, \downarrow\}$ respectively, we finally obtain the electron-hopping Hamiltonian

$$H_{ss} = -t_{ss} \sum_{\sigma} (c_{1,S,\sigma}^\dagger c_{2,S,\sigma} + \text{h.c.}) \quad (\text{A}\cdot 12)$$

between same-parity orbitals (s -orbitals) and the local ASO interaction Hamiltonian

$$H_{sp} = \gamma t_{ss} (c_{1,S,\uparrow}^\dagger c_{2,S,\downarrow} - c_{1,S,\downarrow}^\dagger c_{2,S,\uparrow}) + \text{h.c.} \quad (\text{A}\cdot 13)$$

for different-orbital-parity mixing (s - p orbital mixing), where the ASO coupling constant is given by

$$\gamma = \sqrt{2} \frac{t_{sp}}{t_{ss}} \frac{V_z}{E_s} \frac{\lambda}{\Delta} \quad (\text{A}\cdot 14)$$

in the unit of t_{ss} . As a consequence, in terms of the s -dominant orbital basis, the s - p_x electron transfer is transformed to the ASO interaction. Equation (1) is obtained by the substitutions $\gamma t_{ss} \rightarrow \lambda_A$ and $c_{i,S,\sigma}^\dagger$ ($c_{i,S,\sigma}$) $\rightarrow d_{i\sigma}^\dagger$ ($d_{i\sigma}$) in Eq. (A-13).

Appendix B: Three-Site Hubbard Model for TTQD

Here, we consider the half-filled case of the triangular spin cluster for the strong- U limit using the following three-site Hubbard model Hamiltonian:

$$\begin{aligned} H_{\text{trimer}} &= H_U + H_t \\ &= U \sum_i n_{i\uparrow} n_{i\downarrow} - t \sum_{\sigma} \sum_{i \neq j} d_{i\sigma}^\dagger d_{j\sigma}, \end{aligned} \quad (\text{B}\cdot 1)$$

where i and j ($= a, b, c$) denote the three identical sites with the same electron-hopping matrix element t in H_t . To obtain the lowest-energy states of H_{trimer} , we start from the $t = 0$ case, and next treat a finite- t effect as a perturbation. Owing to the onsite Coulomb interaction term H_U , a single electron is occupied at each site for the lowest-energy states. One of the lowest $S_z = \pm 1/2$ states with $S = 1/2$ is given by

$$|\phi_{\sigma,1}^{E_+}\rangle = \frac{1}{\sqrt{2}} d_{a,\sigma}^\dagger (d_{b,\sigma}^\dagger d_{c,-\sigma}^\dagger - d_{b,-\sigma}^\dagger d_{c,\sigma}^\dagger) |0\rangle, \quad (\text{B}\cdot 2)$$

where E_+ represents an even-parity representation of the degenerate orbitals with the C_3 symmetry⁷²⁾ and the subscript σ of $|\phi_{\sigma,1}^{E_+}\rangle$ represents S_z . On the right-hand side, $-\sigma$ ($= \downarrow, \uparrow$) is the time-reversal component of σ ($= \uparrow, \downarrow$), respectively. In the same manner, the other orbitally degenerate $S_z = \pm 1/2$ state with an odd parity E_- is written as

$$\begin{aligned} |\phi_{\sigma,1}^{E_-}\rangle &= \frac{1}{\sqrt{6}} [2d_{a,-\sigma}^\dagger d_{b,\sigma}^\dagger d_{c,\sigma}^\dagger \\ &\quad - d_{a,\sigma}^\dagger (d_{b,\sigma}^\dagger d_{c,-\sigma}^\dagger + d_{b,-\sigma}^\dagger d_{c,\sigma}^\dagger)] |0\rangle. \end{aligned} \quad (\text{B}\cdot 3)$$

In addition, the $S = 3/2$ states

$$\begin{aligned} |\phi_{3/2}^{A_+}\rangle &= d_{a\uparrow}^\dagger d_{b\uparrow}^\dagger d_{c\uparrow}^\dagger |0\rangle, \quad |\phi_{-3/2}^{A_-}\rangle = d_{a\downarrow}^\dagger d_{b\downarrow}^\dagger d_{c\downarrow}^\dagger |0\rangle, \\ |\phi_{\sigma}^{A_-}\rangle &= \frac{1}{\sqrt{3}} (d_{a,\sigma}^\dagger d_{b,\sigma}^\dagger d_{c,-\sigma}^\dagger + d_{a,\sigma}^\dagger d_{b,-\sigma}^\dagger d_{c,\sigma}^\dagger \\ &\quad + d_{a,-\sigma}^\dagger d_{b,\sigma}^\dagger d_{c,\sigma}^\dagger) |0\rangle \end{aligned} \quad (\text{B}\cdot 4)$$

are categorized into a one-dimensional representation A_- with an odd parity. We note that the E_+ (E_- , A_-) wave function is even (odd) with respect to the interchange of the site indices $b \leftrightarrow c$.

Through the intersite electron hopping, $|\phi_{\sigma,1}^{E_+}\rangle$ is coupled to the doubly occupied states with an excitation energy of U as

$$\begin{cases} |\phi_{\sigma,2}^{E_+}\rangle = \frac{1}{\sqrt{2}} d_{a,\sigma}^\dagger (d_{b,\sigma}^\dagger d_{b,-\sigma}^\dagger + d_{c,\sigma}^\dagger d_{c,-\sigma}^\dagger) |0\rangle, \\ |\phi_{\sigma,3}^{E_+}\rangle = \frac{1}{\sqrt{2}} d_{a,\sigma}^\dagger d_{a,-\sigma}^\dagger (d_{b,\sigma}^\dagger + d_{c,\sigma}^\dagger) |0\rangle, \\ |\phi_{\sigma,4}^{E_+}\rangle = \frac{1}{\sqrt{2}} (d_{b,\sigma}^\dagger d_{b,-\sigma}^\dagger d_{c,\sigma}^\dagger + d_{b,\sigma}^\dagger d_{c,\sigma}^\dagger d_{c,-\sigma}^\dagger) |0\rangle. \end{cases} \quad (\text{B}\cdot 5)$$

In the same manner, $|\phi_{\sigma,1}^{E-}\rangle$ is coupled to

$$\begin{cases} |\phi_{\sigma,2}^{E-}\rangle = \frac{1}{\sqrt{2}}d_{a,\sigma}^\dagger(d_{b,\sigma}^\dagger d_{b,-\sigma}^\dagger - d_{c,\sigma}^\dagger d_{c,-\sigma}^\dagger)|0\rangle, \\ |\phi_{\sigma,3}^{E-}\rangle = \frac{1}{\sqrt{2}}d_{a,\sigma}^\dagger d_{a,-\sigma}^\dagger(d_{b,\sigma}^\dagger - d_{c,\sigma}^\dagger)|0\rangle, \\ |\phi_{\sigma,4}^{E-}\rangle = \frac{1}{\sqrt{2}}(-d_{b,\sigma}^\dagger d_{b,-\sigma}^\dagger d_{c,\sigma}^\dagger + d_{b,\sigma}^\dagger d_{c,\sigma}^\dagger d_{c,-\sigma}^\dagger)|0\rangle. \end{cases} \quad (\text{B}\cdot 6)$$

The 4×4 matrix form of $\langle \phi_{\sigma,i}^{E+} | H_t | \phi_{\sigma,j}^{E+} \rangle$ ($i, j = 1, 2, 3, 4$) is obtained as

$$t \begin{pmatrix} 0 & -2 & 1 & 1 \\ -2 & 0 & 1 & -1 \\ 1 & 1 & -1 & 0 \\ 1 & -1 & 0 & 1 \end{pmatrix}, \quad (\text{B}\cdot 7)$$

and for the E_- states, the H_t matrix is given by

$$t \begin{pmatrix} 0 & 0 & -\sqrt{3} & -\sqrt{3} \\ 0 & 0 & 1 & 1 \\ -\sqrt{3} & 1 & 1 & 0 \\ -\sqrt{3} & 1 & 0 & -1 \end{pmatrix}. \quad (\text{B}\cdot 8)$$

Let us apply the perturbation of H_t to the unperturbed states $|\phi_{\sigma,1}^{E+}\rangle$ and $|\phi_{\sigma,1}^{E-}\rangle$ of H_U . Up to the second order of \bar{t} ($\equiv t/U$), it leads to the following lowest-lying states with the fourfold degeneracy (E_\pm and $\sigma = \uparrow, \downarrow$):⁵⁹⁾

$$\begin{aligned} |\psi_\sigma^{E+}\rangle &= (1 - 3\bar{t}^2)|\phi_{\sigma,1}^{E+}\rangle + 2\bar{t}|\phi_{\sigma,2}^{E+}\rangle \\ &\quad + (-\bar{t} - 3\bar{t}^2)|\phi_{\sigma,3}^{E+}\rangle + (-\bar{t} + 3\bar{t}^2)|\phi_{\sigma,4}^{E+}\rangle, \\ |\psi_\sigma^{E-}\rangle &= (1 - 3\bar{t}^2)|\phi_{\sigma,1}^{E-}\rangle - 2\sqrt{3}\bar{t}^2|\phi_{\sigma,2}^{E-}\rangle \\ &\quad + \sqrt{3}(\bar{t} - \bar{t}^2)|\phi_{\sigma,3}^{E-}\rangle + \sqrt{3}(\bar{t} + \bar{t}^2)|\phi_{\sigma,4}^{E-}\rangle, \end{aligned} \quad (\text{B}\cdot 9)$$

with an energy of $-6t^2/U$.

In Eq. (13), the ASO interaction is introduced in one of the three bonds, i.e., the b - c bond in the triangle cluster, and the corresponding Hamiltonian is given by replacing (1, 2) with (b, c) in Eq. (1). Since the a -site orbital has an even parity ($\tau_z = +1$), the spin-up ($d_{a,\uparrow}^\dagger$) and spin-down ($d_{a,\downarrow}^\dagger$) electron states are categorized into $\tau_z \sigma_z = +1$ and $\tau_z \sigma_z = -1$, respectively. Here, we choose the half-filled states of the $\eta_z = -1$ type $|\psi_\uparrow^{E+}\rangle$, $|\psi_\downarrow^{E-}\rangle$, $|\phi_{3/2}^{A-}\rangle$, and $|\phi_{\downarrow}^{A-}\rangle$: the corresponding S_z values of the total spins are $1/2, -1/2, 3/2$, and $-1/2$, respectively. These four states are coupled to each other through $H_{\text{so}}(b, c)$ as

$$\begin{aligned} \langle \psi_\downarrow^{E-} | H_{\text{so}}(b, c) | \psi_\uparrow^{E+} \rangle &= -\frac{1}{\sqrt{3}}\xi, \\ \langle \phi_{3/2}^{A-} | H_{\text{so}}(b, c) | \psi_\uparrow^{E+} \rangle &= -\frac{1}{\sqrt{2}}\xi, \\ \langle \phi_{\downarrow}^{A-} | H_{\text{so}}(b, c) | \psi_\uparrow^{E+} \rangle &= -\frac{1}{\sqrt{6}}\xi, \end{aligned} \quad (\text{B}\cdot 10)$$

where $\xi = 4\gamma\bar{t}$ and higher-order terms of \bar{t} are neglected.

Here, we show an analogy with the vector spin chirality in the two-site case described in Sect. 2. Let us assume that $|\psi_\uparrow^{E+}\rangle$ has the lowest energy and the other three excited states are almost degenerate, keeping in mind that the E_+ state is stabilized by the Kondo effect in the

TTQD. For $|\psi_\uparrow^{E+}\rangle$, the perturbation of H_{so} in Eq. (B-10) gives the lowest-lying state as

$$\begin{aligned} \alpha |\psi_\uparrow^{E+}\rangle + \beta \left(\frac{1}{\sqrt{3}} |\psi_\downarrow^{E-}\rangle \right. \\ \left. + \frac{1}{\sqrt{2}} |\phi_{3/2}^{A-}\rangle + \frac{1}{\sqrt{6}} |\phi_{\downarrow}^{A-}\rangle \right) \\ \simeq \frac{1}{\sqrt{2}} d_{a\uparrow}^\dagger \left[\alpha (d_{b\uparrow}^\dagger d_{c\downarrow}^\dagger - d_{b\downarrow}^\dagger d_{c\uparrow}^\dagger) \right. \\ \left. + \beta (d_{b\uparrow}^\dagger d_{c\uparrow}^\dagger + d_{b\downarrow}^\dagger d_{c\downarrow}^\dagger) \right] |0\rangle, \end{aligned} \quad (\text{B}\cdot 11)$$

where α and β are real coefficients that satisfy $\alpha^2 + \beta^2 = 1$. The ratio of the matrix elements in Eq. (B-10) is directly reflected in the coefficients of $|\psi_\downarrow^{E-}\rangle$, $|\phi_{3/2}^{A-}\rangle$, and $|\phi_{\downarrow}^{A-}\rangle$. One can find that the vector spin chirality $(\mathbf{S}_b \times \mathbf{S}_c)_y$ is induced by the mixing of the b - c singlet and triplet states in Eq. (B-11), corresponding to $|\phi_S\rangle$ and $-i|\phi_{T_y}\rangle$, respectively, in Eq. (12) in the two-site case.

Appendix C: E_\pm Parity Mixing by Magnetic Flux through TTQD

As well as the ASO interaction, a magnetic flux effect causes the E_\pm orbital-parity mixing between $|\phi_{\sigma,i}^{E+}\rangle$ and $|\phi_{\sigma,j}^{E-}\rangle$ given in Appendix B.⁴³⁾ In this case, the total spin S is conserved. For the equilateral triangle with C_3 symmetry, the electron hopping matrix element of H_t in Eq. (B-1) is modulated by the magnetic flux Φ penetrating through the triangular loop as

$$H_{t,\Phi} = - \sum_{\sigma} \sum_{i \neq j} t e^{i\varphi_{ij}} d_{i\sigma}^\dagger d_{j\sigma}, \quad (\text{C}\cdot 1)$$

where $\varphi_{ab} = \varphi_{bc} = \varphi_{ca} = \varphi/3$ ($\varphi_{ij} = -\varphi_{ji}$) and the phase $\varphi = 2\pi\Phi/\Phi_0$ is defined by the magnetic flux quantum $\Phi_0 = hc/e$ (h : Planck constant, c : speed of light in vacuum, e : elementary charge). The matrix elements of $\langle \phi_{\sigma,i}^{E+} | H_{t,\Phi} | \phi_{\sigma,j}^{E+} \rangle$ and $\langle \phi_{\sigma,i}^{E-} | H_{t,\Phi} | \phi_{\sigma,j}^{E-} \rangle$ ($i, j = 1, 2, 3, 4$) are given by replacing t with $t \cos(\varphi/3)$ in Eqs. (B-7) and (B-8), respectively. For the E_\pm mixing, the 4×4 matrix form of $\langle \phi_{\sigma,i}^{E+} | H_{t,\Phi} | \phi_{\sigma,j}^{E-} \rangle$ is obtained as

$$-it \sin \frac{\varphi}{3} \begin{pmatrix} 0 & -2 & -1 & 1 \\ 0 & 0 & 1 & 1 \\ -\sqrt{3} & -1 & -1 & 0 \\ \sqrt{3} & 1 & 0 & -1 \end{pmatrix}, \quad (\text{C}\cdot 2)$$

and the E_\pm orbital degeneracy is lifted. For a small $|\Phi|$, the off-diagonal matrix element of $H_{t,\Phi}$ is given by

$$\langle \psi_\sigma^{E+} | H_{t,\Phi} | \psi_\sigma^{E-} \rangle \simeq -i6\sqrt{3}\bar{t}^2 t \varphi \quad (\text{C}\cdot 3)$$

on the basis of Eq. (B-9). Thus, the orbital effect of the magnetic field leads to the lowest-energy eigenstates as $|\psi_\sigma^{E+}\rangle \pm i|\psi_\sigma^{E-}\rangle$ for the three-site Hubbard model.

-
- 1) A. C. Hewson, *The Kondo Problem to Heavy Fermions* (Cambridge University Press, Cambridge, U.K., 1993).
 - 2) D. L. Cox and A. Zawadowski, *Adv. Phys.* **47**, 599 (1998).
 - 3) See review articles in *J. Phys. Soc. Jpn.* **74** (2005) (No. 1, Special Topics).

- 4) W. G. van der Wiel, S. De Franceschi, J. M. Elzerman, T. Fujisawa, S. Tarucha, and L. P. Kouwenhoven, *Rev. Mod. Phys.* **75**, 1 (2002).
- 5) P. Jarillo-Herrero, J. Kong, H. S. J. van der Zant, C. Dekker, L. P. Kouwenhoven, and S. De Franceschi, *Nature* **434**, 484 (2005).
- 6) R. Hanson, L. P. Kouwenhoven, J. R. Petta, S. Tarucha, and L. M. K. Vandersypen, *Rev. Mod. Phys.* **79**, 1217 (2007).
- 7) N. Roch, S. Florens, V. Bouchiat, W. Wernsdorfer, and F. Balestro, *Nature* **453**, 633 (2008).
- 8) J. J. Parks, A. R. Champagne, T. A. Costi, W. W. Shum, A. N. Pasupathy, E. Neuscammann, S. Flores-Torres, P. S. Cornaglia, A. A. Alligia, C. A. Balseiro, G. K.-L. Chan, H. D. Abruña, and D. C. Ralph, *Science* **328**, 1370 (2010).
- 9) E. A. Laird, F. Kuemmeth, G. A. Steele, K. Grove-Rasmussen, J. Nygård, K. Flensberg, and L. P. Kouwenhoven, *Rev. Mod. Phys.* **87**, 703 (2015).
- 10) W. Izumida, O. Sakai, and Y. Shimizu, *J. Phys. Soc. Jpn.* **66**, 717 (1997).
- 11) R. López, R. Aguado, and G. Platero, *Phys. Rev. Lett.* **89**, 136802 (2002).
- 12) Y. Tanaka and N. Kawakami, *Phys. Rev. B* **72**, 085304 (2005).
- 13) W.-Z. Wang, *Phys. Rev. B* **83**, 075314 (2011).
- 14) Y. Okazaki, S. Sakai, and K. Muraki, *Phys. Rev. B* **84**, 161305 (2011).
- 15) S. Amasha, A. J. Keller, I. G. Rau, A. Carmi, J. A. Katine, H. Shtrikman, Y. Oreg, and D. Goldhaber-Gordon, *Phys. Rev. Lett.* **110**, 046604 (2013).
- 16) D. Schröer, A. D. Greentree, L. Gaudreau, K. Eberl, L. C. L. Hollenberg, J. P. Kotthaus, and S. Ludwig, *Phys. Rev. B* **76**, 075306 (2007).
- 17) G. Yamahata, Y. Tsuchiya, H. Mizuta, K. Uchida, and S. Oda, *Solid-State Electron.* **53**, 779 (2009).
- 18) S. Amaha, T. Hatano, H. Tamura, S. Teraoka, T. Kubo, Y. Tokura, D. G. Austing, and S. Tarucha, *Phys. Rev. B* **85**, 081301 (2012).
- 19) S. Amaha, W. Izumida, T. Hatano, S. Teraoka, S. Tarucha, J. A. Gupta, and D. G. Austing, *Phys. Rev. Lett.* **110**, 016803 (2013).
- 20) M. Busl, G. Granger, L. Gaudreau, R. Sánchez, A. Kam, M. Pioro-Ladrière, S. A. Studenikin, P. Zawadzki, Z. R. Wasilewski, A. S. Sachrajda, and G. Platero, *Nat. Nanotechnol.* **8**, 261 (2013).
- 21) J. Malecki, *J. Stat. Phys.* **129**, 741 (2007).
- 22) R. Žitko and J. Bonča, *Phys. Rev. B* **84**, 193411 (2011).
- 23) T. Yanagisawa, *J. Phys. Soc. Jpn.* **81**, 094713 (2012).
- 24) M. Zarea, S. E. Ulloa, and N. Sandler, *Phys. Rev. Lett.* **108**, 046601 (2012).
- 25) L. Isaev, D. F. Agterberg, and I. Vekhter, *Phys. Rev. B* **85**, 088107 (2012).
- 26) A. Wong, S. E. Ulloa, N. Sandler, and K. Ingersent, *Phys. Rev. B* **93**, 075148 (2016).
- 27) I. Žutić, J. Fabian, and S. D. Sarma, *Rev. Mod. Phys.* **76**, 323 (2004).
- 28) Y. Ando and M. Shiraishi, *J. Phys. Soc. Jpn.* **86**, 011001 (2017).
- 29) X.-L. Qi and S.-C. Zhang, *Rev. Mod. Phys.* **83**, 1057 (2011).
- 30) Y. Ando, *J. Phys. Soc. Jpn.* **82**, 102001 (2013).
- 31) M. Sato and S. Fujimoto, *J. Phys. Soc. Jpn.* **85**, 072001 (2016).
- 32) Y. Yanase and M. Sigrist, *J. Phys. Soc. Jpn.* **77**, 124711 (2008).
- 33) A. Vidan, R. M. Westervelt, M. Stopa, M. Hanson, and A. C. Gossard, *Appl. Phys. Lett.* **85**, 3602 (2004).
- 34) L. Gaudreau, S. A. Studenikin, A. S. Sachrajda, P. Zawadzki, A. Kam, J. Lapointe, M. Korkusinski, and P. Hawrylak, *Phys. Rev. Lett.* **97**, 036807 (2006).
- 35) M. C. Rogge and R. J. Haug, *Phys. Rev. B* **77**, 193306 (2008).
- 36) S. Amaha, T. Hatano, T. Kubo, S. Teraoka, Y. Tokura, S. Tarucha, and D. G. Austing, *Appl. Phys. Lett.* **94**, 092103 (2009).
- 37) M. Seo, H. K. Choi, S.-Y. Lee, N. Kim, Y. Chung, H.-S. Sim, V. Umansky, and D. Mahalu, *Phys. Rev. Lett.* **110**, 046803 (2013).
- 38) S. Amaha, T. Hatano, S. Teraoka, A. Shibatomi, S. Tarucha, Y. Nakata, T. Miyazawa, T. Oshima, T. Usuki, and N. Yokoyama, *Appl. Phys. Lett.* **92**, 202109 (2008).
- 39) T. Kuzmenko, K. Kikoin, and Y. Avishai, *Phys. Rev. Lett.* **96**, 046601 (2006).
- 40) A. Oguri, Y. Nisikawa, Y. Tanaka, and T. Numata, *J. Magn. Magn. Mater.* **310**, 1139 (2007).
- 41) W.-Z. Wang, *Phys. Rev. B* **76**, 115114 (2007).
- 42) R. Žitko and J. Bonča, *Phys. Rev. B* **77**, 245112 (2008).
- 43) W.-Z. Wang, *Phys. Rev. B* **78**, 235316 (2008).
- 44) A. K. Mitchell, T. F. Jarrold, and D. E. Logan, *Phys. Rev. B* **79**, 085124 (2009).
- 45) E. Vernek, C. A. Büsser, G. B. Martins, E. V. Anda, N. Sandler, and S. E. Ulloa, *Phys. Rev. B* **80**, 035119 (2009).
- 46) A. Oguri, S. Amaha, Y. Nishikawa, T. Numata, M. Shimamoto, A. C. Hewson, and S. Tarucha, *Phys. Rev. B* **83**, 205304 (2011).
- 47) A. K. Mitchell, T. F. Jarrold, M. R. Galpin, and D. E. Logan, *J. Phys. Chem. B* **117**, 12777 (2013).
- 48) S. B. Tooski, B. R. Bulka, R. Žitko, and A. Ramšak, *Eur. Phys. J. B* **87**, 145 (2014).
- 49) A. Oguri, I. Sato, M. Shimamoto, and Y. Tanaka, *J. Phys.: Conf. Ser.* **592**, 012143 (2015).
- 50) Y.-C. Xiong, W.-Z. Wang, S.-J. Luo, J.-T. Yang, and H.-M. Huang, *J. Magn. Magn. Mater.* **399**, 5 (2016).
- 51) S. B. Tooski, A. Ramšak, and B. R. Bulka, *Physica E* **75**, 345 (2016).
- 52) H. Akera, *Phys. Rev. B* **47**, 6835 (1993).
- 53) C. Bruder, R. Fazio, and H. Schoeller, *Phys. Rev. Lett.* **76**, 114 (1996).
- 54) W. Hofstetter, J. König, and H. Schoeller, *Phys. Rev. Lett.* **87**, 156803 (2001).
- 55) Y. Tanaka and N. Kawakami, *J. Phys. Soc. Jpn.* **75**, 015004 (2006).
- 56) Y. Komijani, R. Yoshii, and I. Affleck, *Phys. Rev. B* **88**, 245104 (2013).
- 57) M. Koga, M. Matsumoto, and H. Kusunose, *J. Phys. Soc. Jpn.* **81**, 123703 (2012); M. Koga, M. Matsumoto, and H. Kusunose, *J. Phys. Soc. Jpn.* **82**, 093706 (2013); M. Koga, M. Matsumoto, and H. Kusunose, *JPS Conf. Proc.* **3**, 012020 (2014).
- 58) M. Koga, M. Matsumoto, and H. Kusunose, *J. Phys. Soc. Jpn.* **85**, 063702 (2016).
- 59) L. N. Bulaevskii, C. D. Batista, M. V. Mostovoy, and D. I. Khomskii, *Phys. Rev. B* **78**, 024402 (2008).
- 60) M. Koga, M. Matsumoto, and H. Kusunose, *J. Phys. Soc. Jpn.* **83**, 084707 (2014); M. Koga, M. Matsumoto, and H. Kusunose, *J. Phys.: Conf. Ser.* **592**, 012142 (2015).
- 61) K. G. Wilson, *Rev. Mod. Phys.* **47**, 773 (1975).
- 62) H. R. Krishna-murthy, J. W. Wilkins, and K. G. Wilson, *Phys. Rev. B* **21**, 1003 (1980); H. R. Krishna-murthy, J. W. Wilkins, and K. G. Wilson, *Phys. Rev. B* **21**, 1044 (1980).
- 63) R. Bulla, T. A. Costi, and T. Pruschke, *Rev. Mod. Phys.* **80**, 395 (2008).
- 64) Y. Yanase and H. Harima, private communication.
- 65) The Hamiltonian H_{dimer} in Eq. (6) is invariant under the following two symmetry operations: (a) the mirror operation represented by $\sigma_v = \tau_z \sigma_x$, whose normal is perpendicular to the x axis defined in deriving Eq. (A-13), and (b) the time-reversal operation expressed as $T = -i\sigma_y K$, where the operator K for a complex conjugate can be omitted in the present analysis. Notice that H_{dimer} is also invariant under another operation $\tau_z \sigma_z (\equiv \sigma_v \otimes T)$, which means that the above two symmetry operations are performed simultaneously. Throughout the paper, we use η_z in Eq. (5) to classify wave functions.
- 66) Here, the vector spin chirality operator is defined as $(\mathbf{S}_1 \times \mathbf{S}_2)_\alpha = -(i/2)(|\phi_{T_\alpha}\rangle\langle\phi_S| - |\phi_S\rangle\langle\phi_{T_\alpha}|)$, where the singlet state $|\phi_S\rangle$ is given in Eq. (7) and the triplet states $|\phi_{T_\alpha}\rangle$ ($\alpha = x, y, z$) are $|\phi_{T_x}\rangle = (1/\sqrt{2})(-d_{1\uparrow}^\dagger d_{2\uparrow}^\dagger + d_{1\downarrow}^\dagger d_{2\downarrow}^\dagger)|0\rangle$, $|\phi_{T_y}\rangle = (i/\sqrt{2})(d_{1\uparrow}^\dagger d_{2\uparrow}^\dagger + d_{1\downarrow}^\dagger d_{2\downarrow}^\dagger)|0\rangle$, and $|\phi_{T_z}\rangle = (1/\sqrt{2})(d_{1\uparrow}^\dagger d_{2\downarrow}^\dagger + d_{1\downarrow}^\dagger d_{2\uparrow}^\dagger)|0\rangle$, which are named after the relationship between the p -orbital wave functions and the $l = 1$ angular momentum in Eqs. (A-1)–(A-3).
- 67) M. Matsumoto, K. Chimata, and M. Koga, *J. Phys. Soc. Jpn.* **86**, 034704 (2017).
- 68) S. Fölsch, J. Martínez-Blanco, J. Yang, K. Kanisawa, and S.

- C. Erwin, Nat. Nanotechnol. **9**, 505 (2014).
- 69) A. J. Heinrich, J. A. Gupta, C. P. Lutz, and D. M. Eigler, Science **306**, 466 (2004).
- 70) C. F. Hirjibehedin, C. P. Lutz, and A. J. Heinrich, Science **312**, 1021 (2006).
- 71) R. Wiesendanger, Rev. Mod. Phys. **81**, 1495 (2009).
- 72) C. Janani, J. Merino, I. P. McCulloch, and B. J. Powell, Phys. Rev. Lett. **113**, 267204 (2014).